

CGC/saturation approach for soft interactions at high energy: long range rapidity correlations

E. Gotsman,^a E. Levin^{a,b} and U. Maor^a

^a*Department of Particle Physics, School of Physics and Astronomy, Raymond and Beverly Sackler Faculty of Exact Science, Tel Aviv University, Tel Aviv, 69978, Israel*

^b*Departamento de Física, Universidad Técnica Federico Santa María, and Centro Científico-Tecnológico de Valparaíso, Avda. España 1680, Casilla 110-V, Valparaíso, Chile*

E-mail: gotsman@post.tau.ac.il, leving@post.tau.ac.il, eugeny.levin@usm.cl,
maor@post.tau.ac.il

ABSTRACT: In this paper we continue our program to build a model for high energy soft interactions, that is based on the CGC/saturation approach. The main result of this paper is that we have discovered a mechanism that leads to large long range rapidity correlations, and results in large values of the correlation function $R(y_1, y_2) \geq 1$, which is independent of y_1 and y_2 . Such behaviour of the correlation function, provides strong support for the idea, that at high energies the system of partons that is produced, is not only dense, but also has strong attractive forces acting between the partons.

KEYWORDS: BFKL Pomeron, soft interaction, CGC/saturation approach, correlations

Contents

1	Introduction	1
2	Our model: generalities, elastic amplitude and inclusive production	2
3	Two particle correlations	6
3.1	Correlations between two parton showers	6
3.2	Correlations in one parton shower: semi-enhanced diagrams	7
3.3	Correlations in one parton shower: enhanced diagrams	10
3.4	Correlation function	11
3.5	Kinematic corrections	12
3.6	Correlation in one parton shower: emission from one BFKL Pomeron	12
3.7	Short range rapidity correlation	14
4	Predictions and comparison with the experiment	14
5	Conclusion	19
6	Acknowledgements	19

1 Introduction

The large body of experimental data on soft interactions at high energy[1–9], presently, cannot be comprehended in terms of theoretical high energy QCD (see [10] for the review).

In this paper we continue our effort[11–13] to comprehend such interactions, by constructing a model that incorporates the advantages of two theoretical approaches to high energy QCD.

The first one is the CGC/saturation approach [14–20], which provides a clear picture of multi particle production at high energy, that proceeds in two stages. The first stage is the production of a mini-jet with the typical transverse momentum Q_s . Where Q_s the saturation scale, is much larger than the soft scale. This stage is under full theoretical control. The second stage is when the mini-jet decays into hadrons, which we have to treat phenomenologically, using data from hard processes. Such an approach leads to a good

description of the experimental data on inclusive production, both for hadron-hadron, hadron-nucleus and nucleus-nucleus collisions, and the observation of some regularities in the data, such as geometric scaling behaviour[21–25]. The shortcoming of this approach is, the fact that it is disconnected from diffractive physics.

On the other hand, there exists a different approach to high energy QCD: the BFKL Pomeron[26] and its interactions[14, 28–35], which is suitable to describe diffractive physics. The BFKL Pomeron calculus turns out to be close to the old Reggeon theory [36], so for calculating the inclusive characteristics of multiparticle production, we can apply the Mueller diagram technique[37]. The relation between these two approaches has not yet been established, but they are equivalent[34] for the rapidities ($\ln(s/s_0)$), such that

$$Y \leq \frac{2}{\Delta_{\text{BFKL}}} \ln \left(\frac{1}{\Delta_{\text{BFKL}}^2} \right) \quad (1.1)$$

where Δ_{BFKL} denotes the intercept of the BFKL Pomeron. As we have discussed [11], the parameters of our model are such that for $Y \leq 36$, we can trust our approach, based on the BFKL Pomeron calculus.

This paper is the next step in our program to build a model for high energy soft scattering, based on an analytical calculation, without using a Monte Carlo simulation. We discuss the correlation function:

$$R(y_1, y_2; Y) = \frac{1}{\sigma_{NSD}} \frac{d^2\sigma}{dy_1 dy_2} \bigg/ \left(\frac{1}{\sigma_{NSD}} \frac{d\sigma}{dy_1} \frac{1}{\sigma_{NSD}} \frac{d\sigma}{dY_2} \right) - 1 \quad (1.2)$$

where Y denotes the total rapidity ($Y = \ln(s/s_0)$ and $s = W^2$, W is the energy in c.m.f.) and y_1 and y_2 are the rapidities of the produced hadrons. $\sigma_{NSD} = \sigma_{tot} - \sigma_{el} - \sigma_{sd} - \sigma_{dd}$ where $\sigma_{tot}(\sigma_{el}, \sigma_{sd}, \sigma_{dd})$ are total, elastic, single and double diffraction cross sections.

The paper is organized as follows. In the following section we discuss the main features of our approach, concentrating on the description of diffractive processes. In section 3, we derive the main formulae for the correlation functions in our approach, while in section 4 we compare our predictions with the available experimental data.

2 Our model: generalities, elastic amplitude and inclusive production

In this section we briefly review our model, which successfully describes diffractive[11, 12] and inclusive cross sections[13]. The main ingredient of our model is the BFKL Pomeron Green's function, which we determined using the CGC/saturation approach[11, 35]. We determined this function from the solution of the non-linear Balitsky-Kovchegov equation[17, 19], using the MPSI approximation[38] to sum enhanced diagrams shown in Fig. 1-a. It has the following form:

$$\begin{aligned} G^{\text{dressed}}(T) &= a^2(1 - \exp(-T)) + 2a(1 - a) \frac{T}{1 + T} + (1 - a)^2 G(T) \\ \text{with } G(T) &= 1 - \frac{1}{T} \exp\left(\frac{1}{T}\right) \Gamma_0\left(\frac{1}{T}\right) \end{aligned} \quad (2.1)$$

$$T(s, b) = \phi_0 S(b, m) e^{0.63\lambda \ln(s/s_0)} \quad \text{with} \quad S(b, m) = \frac{m^2}{2\pi} e^{-mb} \quad (2.2)$$

In these formulae we take $a = 0.65$, this value was chosen, so as to obtain the analytical form for the solution of the BK equation. Parameters λ and ϕ_0 , can be estimated in the leading order of QCD, but due to large next-to-leading order corrections, we treat them as parameters of the fit. m is a non-perturbative parameter, which characterize the large impact parameter behavior of the saturation momentum, as well as the typical sizes of dipoles that take part in the interactions. The value of $m = 5.25 \text{ GeV}$ in our model, justifies our main assumption, that BFKL Pomeron calculus based on a perturbative QCD approach, is able to describe soft physics, since $m \gg \mu_{soft}$, where μ_{soft} denotes the natural scale for soft processes ($\mu_{soft} \sim \Lambda_{QCD}$ and/or pion mass).

Unfortunately, since the confinement problem is far from being solved, we assume a phenomenological approach for the structure of the colliding hadron. We use a two channel model, which allows us to calculate the diffractive production in the region of small masses. In this model, we replace the rich structure of the diffractively produced states, by a single state with the wave function ψ_D , a la Good-Walker[39]. The observed physical hadronic and diffractive states are written in the form

$$\psi_h = \alpha \Psi_1 + \beta \Psi_2; \quad \psi_D = -\beta \Psi_1 + \alpha \Psi_2; \quad \text{where} \quad \alpha^2 + \beta^2 = 1; \quad (2.3)$$

Functions ψ_1 and ψ_2 form a complete set of orthogonal functions $\{\psi_i\}$ which diagonalize the interaction matrix \mathbf{T}

$$A_{i,k}^{i'k'} = \langle \psi_i \psi_k | \mathbf{T} | \psi_{i'} \psi_{k'} \rangle = A_{i,k} \delta_{i,i'} \delta_{k,k'}. \quad (2.4)$$

The unitarity constraints take the form

$$2 \text{Im} A_{i,k}(s, b) = |A_{i,k}(s, b)|^2 + G_{i,k}^{in}(s, b), \quad (2.5)$$

where $G_{i,k}^{in}$ denotes the contribution of all non diffractive inelastic processes, i.e. it is the summed probability for these final states to be produced in the scattering of a state i off a state k . In Eq. (2.5) $\sqrt{s} = W$ denotes the energy of the colliding hadrons, and b the impact parameter. A simple solution to Eq. (2.5) at high energies, has the eikonal form with an arbitrary opacity Ω_{ik} , where the real part of the amplitude is much smaller than the imaginary part.

$$A_{i,k}(s, b) = i (1 - \exp(-\Omega_{i,k}(s, b))), \quad (2.6)$$

$$G_{i,k}^{in}(s, b) = 1 - \exp(-2\Omega_{i,k}(s, b)). \quad (2.7)$$

Eq. (2.7) implies that $P_{i,k}^S = \exp(-2\Omega_{i,k}(s, b))$, is the probability that the initial projectiles (i, k) reach the final state interaction unchanged, regardless of the initial state re-scatterings.

Note, that there is no factor $1/2$, its absence stems from our definition of the dressed Pomeron.

In the eikonal approximation we replace $\Omega_{i,k}(s, b)$ by

$$\Omega_{i,k}(s, b) = \int d^2b' d^2b'' g_i(\vec{b}') G^{\text{dressed}}(T(s, \vec{b}'')) g_k(\vec{b} - \vec{b}' - \vec{b}'') \quad (2.8)$$

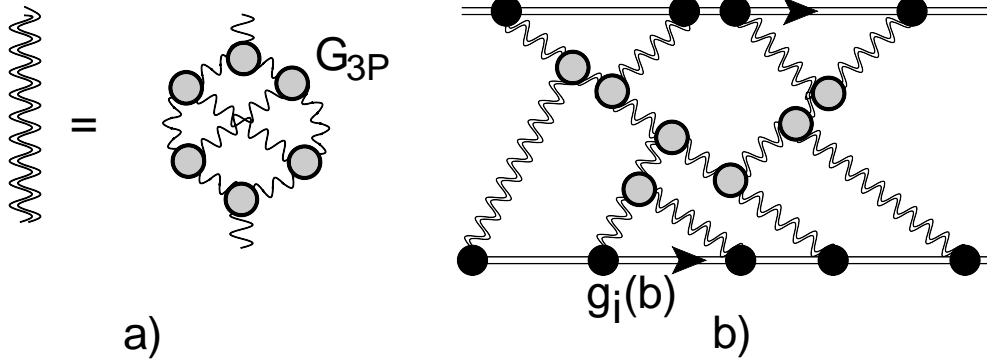


Figure 1. Fig. 1-a shows the set of the diagrams in BFKL Pomeron calculus. The wavy double lines denote the resulting (dressed) Green's function of the Pomeron in the framework of high energy QCD, while the single wavy lines describe the BFKL Pomerons. In Fig. 1-b we show the net diagrams that include the interaction of BFKL Pomerons with colliding hadrons.

model	λ	ϕ_0 (GeV^{-2})	g_1 (GeV^{-1})	g_2 (GeV^{-1})	m (GeV)	m_1 (GeV)	m_2 (GeV)	β	a_{PP}
2 channel	0.38	0.0019	110.2	11.2	5.25	0.92	1.9	0.58	0.21

Table 1. Fitted parameters of the model. The values are taken from Ref.[12].

We propose a more general approach, which takes into account new small parameters, that come from the fit to the experimental data (see Table 1 and Fig. 1):

$$G_{3P}/g_i(b=0) \ll 1; \quad m \gg m_1 \text{ and } m_2 \quad (2.9)$$

The second equation in Eq. (2.9) leads to the fact that b'' in Eq. (2.8) is much smaller than b and b' therefore, Eq. (2.8) can be re-written in a simpler form

$$\begin{aligned} \Omega_{i,k}(s, b) &= \left(\int d^2b'' G^{\text{dressed}}(T(s, \vec{b}'')) \right) \int d^2b' g_i(\vec{b}') g_k(\vec{b} - \vec{b}') \\ &= \tilde{G}^{\text{dressed}}(\bar{T}) \int d^2b' g_i(\vec{b}') g_k(\vec{b} - \vec{b}') \end{aligned} \quad (2.10)$$

Selecting the diagrams using the first equation in Eq. (2.9), indicates that the main contribution stems from the net diagrams shown in Fig. 1-b. The sum of these diagrams[12] leads to the following expression for $\Omega_{i,k}(s, b)$

$$\Omega(Y; b) = \int d^2b' \frac{g_i(\vec{b}') g_k(\vec{b} - \vec{b}') \tilde{G}^{\text{dressed}}(T)}{1 + G_{3P} \tilde{G}^{\text{dressed}}(T) [g_i(\vec{b}') + g_k(\vec{b} - \vec{b}')]}; \quad (2.11)$$

$$g_i(b) = g_i S_p(b; m_i); \quad (2.12)$$

where

$$S_p(b, m_i) = \frac{1}{4\pi} m_i^3 b K_1(m_i b)$$

$$\tilde{G}^{\text{dressed}}(\bar{T}) = \int d^2b G^{\text{dressed}}(T(s, b))$$

where $T(s, b)$ is given by Eq. (2.2).

Note that $\tilde{G}^{\text{dressed}}(\bar{T})$ does not depend on b and is a function of $\bar{T} = T(s, b = 0) = \phi_0 e^{0.63 \lambda Y}$.

In all previous formulae, the value of the triple BFKL Pomeron vertex is known: $G_{3P} = 1.29 \text{ GeV}^{-1}$.

To simplify further discussion, we introduce the notation

$$N^{BK}(G_{\mathbb{P}}^i(Y, b)) = a(1 - \exp(-G_{\mathbb{P}}^i(Y, b))) + (1 - a) \frac{G_{\mathbb{P}}^i(Y, b)}{1 + G_{\mathbb{P}}^i(Y, b)}, \quad (2.13)$$

with $a = 0.65$. Eq. (2.13) is an analytical approximation to the numerical solution for the BK equation[35]. $G_{\mathbb{P}}(Y; b) = g_i(b) \tilde{G}^{\text{dressed}}(\bar{T})$. We recall that the BK equation sums the ‘fan’ diagrams shown in Fig. 2.

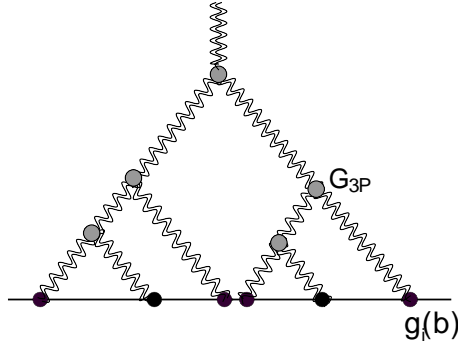


Figure 2. A typical example of ‘fan’ diagrams that are summed in Eq. (2.13).

For the elastic amplitude we have

$$a_{el}(b) = (\alpha^4 A_{1,1} + 2\alpha^2 \beta^2 A_{1,2} + \beta^4 A_{2,2}). \quad (2.14)$$

To determine the correlation function (given in Eq. (1.2)), we need to know the single inclusive cross sections. We have discussed these cross sections in Ref.[13], for the sake of completeness we give the formula that describes the Mueller diagram of Fig. 3.

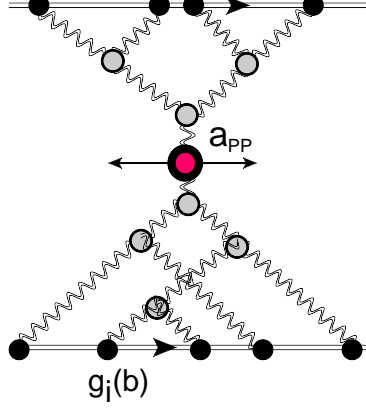


Figure 3. Mueller diagram for the single inclusive cross section. The double wavy lines describe the resulting Green's function of the BFKL Pomerons ($\tilde{G}^{\text{dressed}}$). The blobs stand for the vertices which are the same as in Fig. 1.

$$\begin{aligned}
\frac{d\sigma}{dy} &= \int d^2p_T \frac{d\sigma}{dy d^2p_T} = a_{PP} \ln(W/W_0) \left\{ \alpha^4 In^{(1)}\left(\frac{1}{2}Y + y\right) In^{(1)}\left(\frac{1}{2}Y - y\right) \right. \\
&+ \alpha^2 \beta^2 \left(In^{(1)}\left(\frac{1}{2}Y + y\right) In^{(2)}\left(\frac{1}{2}Y - y\right) + In^{(2)}\left(\frac{1}{2}Y + y\right) In^{(1)}\left(\frac{1}{2}Y - y\right) \right) \\
&\left. + \beta^4 In^{(2)}\left(\frac{1}{2}Y + y\right) In^{(2)}\left(\frac{1}{2}Y - y\right) \right\}
\end{aligned} \tag{2.15}$$

where Y denotes the total rapidity of the colliding particles, and y is the rapidity of produced hadron. $In^{(i)}$ is given by

$$In^{(i)}(y) = \int d^2b N^{BK} \left(g^{(i)} S(m_i, b) \tilde{G}_P(y) \right) \tag{2.16}$$

a_{PP} is a fitted parameter, that was determined in Ref.[13] (see Table 1).

3 Two particle correlations

3.1 Correlations between two parton showers

The Mueller diagram for the correlations between two parton showers is shown in Fig. 4. Examining this diagram, we see that the contribution to the double inclusive cross section, differs from the product of two single inclusive cross sections. There are two reasons for this, the first, is that in the expression for the double inclusive cross section, we integrate the product of the single inclusive inclusive cross sections, over

b , at fixed b . The second, is that the summation over i and k for the product of single inclusive cross sections, is for fixed i and k .

Introducing the following new function, enables us to write the analytical expression:

$$I^{(i,k)}(y, b) = a_{PP} \ln(W/W_0) \quad (3.1)$$

$$\times \int d^2b' N^{BK} \left(g^{(i)} S(m_i, b') \tilde{G}^{\text{dressed}} \left(\frac{1}{2}Y + y \right) \right) N^{BK} \left(g^{(k)} S(m_k, \vec{b} - \vec{b}') \tilde{G}^{\text{dressed}} \left(\frac{1}{2}Y - y \right) \right)$$

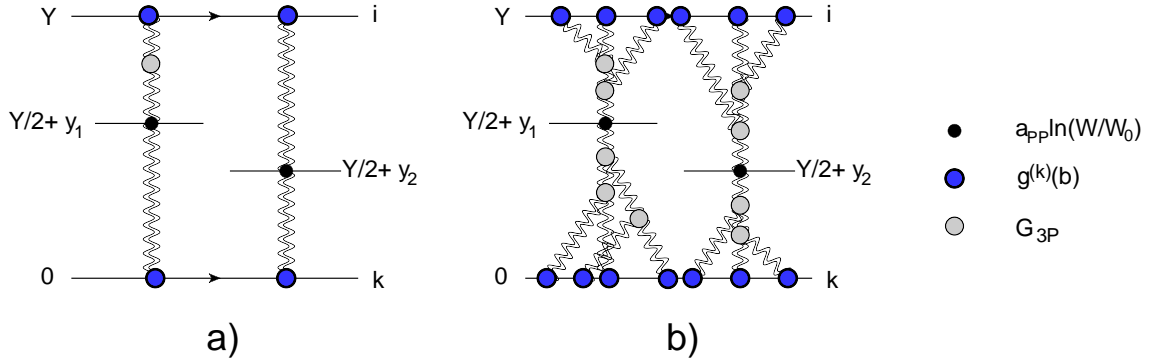


Figure 4. The Mueller diagram for the rapidity correlation between two particles produced in two parton showers. Fig. 4-a shows the first Mueller diagram, while Fig. 4-b indicates the structure of general diagrams. The double wavy lines describe the dressed BFKL Pomerons. The blobs stand for the vertices as shown in the legend.

Using Eq. (3.1) we can write the double inclusive cross section in the form

$$\frac{d^2 \sigma^{\text{parton showers}}}{dy_1 dy_2} = \int d^2b \left\{ \alpha^4 I^{(1,1)}(y_1, b) I^{(1,1)}(y_2, b) \right. \quad (3.2)$$

$$\left. \alpha^2 \beta^2 \left(I^{(1,2)}(y_1, b) I^{(1,2)}(y_2, b) + I^{(2,1)}(y_1, b) I^{(2,1)}(y_2, b) \right) + \beta^4 I^{(2,2)}(y_1, b) I^{(2,2)}(y_2, b) \right\}$$

Comparing Eq. (3.2) with Eq. (2.15) squared, we note the different powers of α and β , which reflect the different summation over i and k , as well as different integration over b .

3.2 Correlations in one parton shower: semi-enhanced diagrams

The main theoretical assumption that we make in calculating the correlation in a one parton shower, is that the Mueller diagram technique [37], and the AGK cutting rules[40] are valid. We should note, however, that even if the Mueller diagrams provide the correct description of inclusive processes in QCD, the AGK cutting rules are not valid for calculations of the correlations in QCD [41, 42]. Nevertheless, we believe that, we can neglect the AGK cutting rules violating contributions since, first, they do not lead to long range rapidity correlations, which are the main subject of our concern, and second, as we will show below, the correlations in one parton shower turn out to be negligibly small.

It is instructive to write the expression for the first Mueller diagram in the following form (see

$$\begin{aligned} \frac{d^2\sigma_{\text{one parton shower}}}{dy_1 dy_2} &= (a_{\mathbb{P}\mathbb{P}} \ln(W/W_0))^2 \sum_{i=1,k=1}^2 \alpha_i^2 \alpha_k^2 \int_{\max(\frac{1}{2}Y-y_1, \frac{1}{2}Y-y_2)}^Y dY' \\ &\int d^2b g_i(b) \tilde{G}(Y-Y') G_{3\mathbb{P}} \tilde{G}\left(Y' - \frac{1}{2}Y - y_1\right) \tilde{G}\left(Y' - \frac{1}{2}Y - y_2\right) \\ &\int d^2b' N^{BK}\left(g^k(b) \tilde{G}\left(\frac{1}{2}Y - y_1\right)\right) \int d^2b' N^{BK}\left(g^k(b) \tilde{G}\left(\frac{1}{2}Y - y_2\right)\right) \end{aligned} \quad (3.3)$$

The expression for the first Mueller diagram for two parton showers correlation (see Fig. 4-a) has the form

$$\begin{aligned} \frac{d^2\sigma_{\text{two parton showers}}}{dy_1 dy_2} &= \int d^2b \frac{d^2\sigma^2 \text{ parton showers}}{dy_1 dy_2 d^2b} = \\ &(a_{\mathbb{P}\mathbb{P}} \ln(W/W_0))^2 \sum_{i=1,k=1}^2 \alpha_i^2 \alpha_k^2 \int d^2b (g_i(b))^2 \tilde{G}\left(Y' - \frac{1}{2}Y - y_1\right) \tilde{G}\left(Y' - \frac{1}{2}Y - y_2\right) \\ &\int d^2b' N^{BK}\left(g^k(b) \tilde{G}\left(\frac{1}{2}Y - y_1\right)\right) \int d^2b' N^{BK}\left(g^k(b) \tilde{G}\left(\frac{1}{2}Y - y_2\right)\right) \end{aligned} \quad (3.4)$$

Comparing Eq. (3.3) with Eq. (3.4) one can see that

$$\begin{aligned} \frac{d^2\sigma_{\text{one parton shower}}}{dy_1 dy_2} &= \mathcal{H}(Y, y_1, y_2) \int d^2b \frac{G_{3\mathbb{P}}}{g_1(b)} \frac{d^2\sigma^2 \text{ parton showers}}{dy_1 dy_2 d^2b} \\ \mathcal{H}(Y, y_1, y_2) &= \int_{\max(\frac{1}{2}Y-y_1, \frac{1}{2}Y-y_2)}^Y dY' \frac{\tilde{G}(Y-Y') \tilde{G}(Y' - \frac{1}{2}Y - y_1) \tilde{G}(Y' - \frac{1}{2}Y - y_2)}{\tilde{G}(\frac{1}{2}Y - y_1) \tilde{G}(\frac{1}{2}Y - y_2)} \end{aligned} \quad (3.5)$$

$\mathcal{H}(Y, y_1, y_2)$ is proportional to $\frac{1}{2}Y - y_1 (y_1 > y_2)$ in the kinematic region where $\tilde{G}(Y)$ is a constant. At small Y it is a constant and is equal to $\int d^2b T(Y=0, b) / \Delta$, where $\Delta = 0.63\lambda$. Therefore, we can expect that the semi-enhanced diagrams can give larger contribution to the double inclusive cross section than the production from two parton showers. However, Fig. 5 shows that both the value, and the increase turns out to be small in the kinematic region accessible to experiment. Even at ultra high energies, shown in Fig. 5-b, $\mathcal{H}(Y, y_1, y_2) \leq 0.012$.

On the other hand, the contribution of Eq. (3.5) is small and is proportional to $G_{3\mathbb{P}}/g_i \ll 1$. Bearing in mind that $G_{3\mathbb{P}} = 1.29$ in our approach, one can see that maximum value for $\max(\mathcal{H}) \approx 0.012$ and the values of

$$\max(\mathcal{H}) \frac{G_{3\mathbb{P}}}{g_1(0)} \approx 1.4 \cdot 10^{-4}; \quad \max(\mathcal{H}) \frac{G_{3\mathbb{P}}}{g_2(0)} \approx 1.4 \cdot 10^{-3}; \quad (3.6)$$

Therefore, we expect that the contribution of the correlations due semi-enhanced diagrams, is negligibly small.

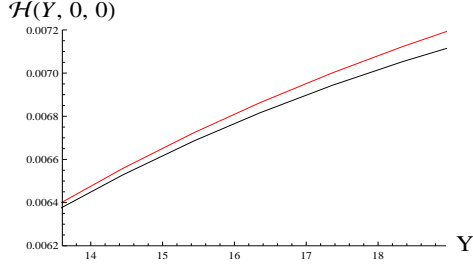


Fig. 5-a

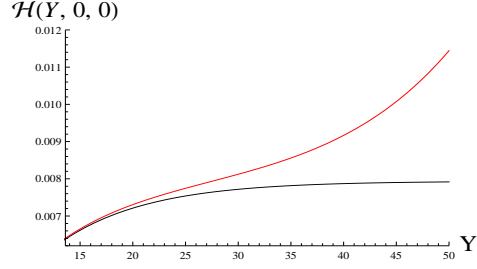


Fig. 5-b

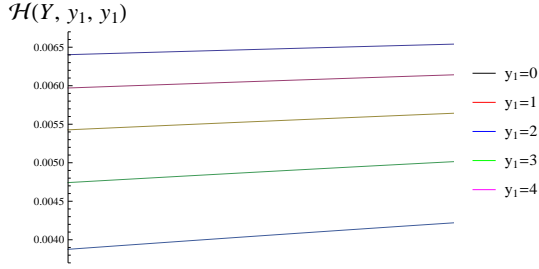


Fig. 5-c

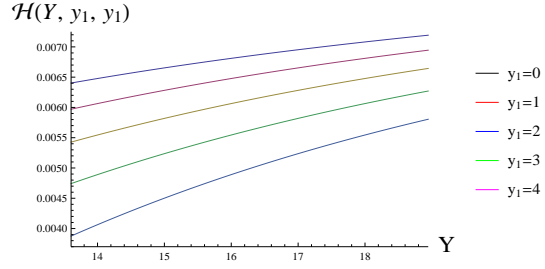


Fig. 5-d

Figure 5. Fig. 5-a: The function $\mathcal{H}(Y, y_1, y_2)$ versus $Y = \ln(W^2/W_0^2)$ for $y_1 = y_2 = 0$. The curve 1 shows $\mathcal{H}(Y, y_1, y_2)$ in which all \tilde{G} are replaced by the first order of its expansion with respect to $T(Y, b)$; line 2 is the exact calculation. Fig. 5-b is the same as Fig. 5-a but for a large region of Y . In Fig. 5-c $\mathcal{H}(Y, y_1, y_1)$ is plotted versus Y at different values of y_1 . $\mathcal{H}(Y, 0, y_2)$ is shown in Fig. 5-d as function of $|y_2|$ at different energies W .

The general expression for the double inclusive cross section (see Fig. 6-b) can be written using two new functions $S^i(y_1, y_2)$ and $S_k(y_1, y_2)$ defined as

$$S^i(y_1, y_2) = \int d^2b' N^{BK} \left(g^{(i)} S(m_i, b') \tilde{G}^{\text{dressed}} \left(\frac{1}{2}Y + y_1 \right) \right) N^{BK} \left(g^{(i)} S(m_i, b') \tilde{G}^{\text{dressed}} \left(\frac{1}{2}Y + y_2 \right) \right) \times \left(\frac{G_{3P}}{g^{(i)} S(m_i, b')} \right) \quad (3.7)$$

$$S_i(y_1, y_2) = \int d^2b' N^{BK} \left(g^{(i)} S(m_i, b') \tilde{G}^{\text{dressed}} \left(\frac{1}{2}Y - y_1 \right) \right) N^{BK} \left(g^{(i)} S(m_i, b') \tilde{G}^{\text{dressed}} \left(\frac{1}{2}Y - y_2 \right) \right) \quad (3.8)$$

It takes the form

$$\frac{d^2\sigma_{\text{semi-enhanced}}^{\text{1 parton shower}}}{dy_1 dy_2} = \mathcal{H}(Y, y_1, y_2) (a_{PP} \ln(W/W_0))^2 \left\{ 2\alpha^4 S^1(y_1, y_2) S_1(y_1, y_2) + \alpha^2 \beta^2 (S^1(y_1, y_2) S_2(y_1, y_2) + S_1(-y_1, -y_2) S^2(-y_1, -y_2)) + 2\beta^4 S^2(y_1, y_2) S_2(y_1, y_2) \right\} \quad (3.9)$$

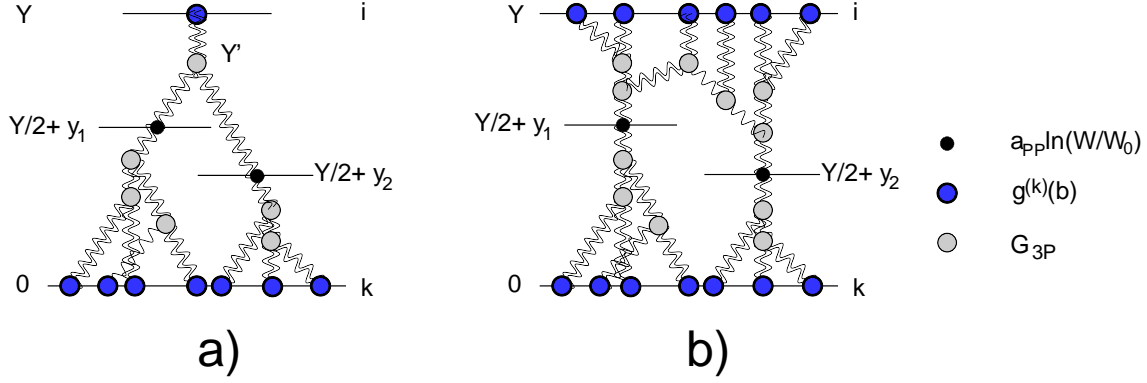


Figure 6. Mueller diagrams for the rapidity correlation between two particles produced in one parton showers: semi-enhanced diagrams. Fig. 6-a shows the first Mueller diagram, while Fig. 6-b gives the structure of general diagrams. The double wavy lines describe dressed BFKL Pomerons. The blobs stand for the vertices shown in the legend

3.3 Correlations in one parton shower: enhanced diagrams

The first Mueller diagram for the correlations from the enhanced diagram is shown in Fig. 7 -a, and has the following form

$$\begin{aligned}
 \frac{d^2 \sigma_{enh}^{one\ parton\ shower}}{dy_1 dy_2} &= (a_{PP} \ln(W/W_0))^2 \sum_{i=1, k=1}^2 \alpha_i^2 \alpha_k^2 \int_{\max(\frac{1}{2}Y-y_1, \frac{1}{2}Y-y_2)}^Y dY' \int_0^{\min(\frac{1}{2}Y-y_1, \frac{1}{2}Y-y_2)} dY'' \\
 &\int d^2b g_i(b) \tilde{G}(Y-Y') G_{3P} \tilde{G}\left(Y' - \frac{1}{2}Y - y_1\right) \tilde{G}\left(Y' - \frac{1}{2}Y - y_2\right) \\
 &, \int d^2b' g_k(b') \tilde{G}\left(\frac{1}{2}Y + y_2 - Y''\right) \tilde{G}\left(\frac{1}{2}Y + y_1 - Y''\right) G_{3P} \tilde{G}(Y'')
 \end{aligned} \tag{3.11}$$

this can be re-written as

$$\frac{d^2 \sigma_{enh}^{one\ parton\ shower}}{dy_1 dy_2} = \int d^2b \frac{G_{3P}}{g_i(b)} \frac{G_{3P}}{g_k(b)} \frac{d^2 \sigma^{2\ parton\ showers}}{dy_1 dy_2 d^2b} \tag{3.12}$$

An example of typical diagrams is shown in Fig. 7. The formula, summing all diagrams shown in

Fig. 7-b takes the form

$$\frac{d^2 \sigma_{\text{enhanced}}^{\text{1 parton shower}}}{dy_1 dy_2} = \mathcal{K} (a_{\mathbb{P}\mathbb{P}} \ln(W/W_0))^2 \mathcal{H}(Y, y_1, y_2) \mathcal{H}(Y, -y_1, -y_2) \quad (3.13)$$

$$\left\{ \alpha^4 S^1(y_1, y_2) S^1(-y_1, -y_2) + \alpha^2 \beta^2 \left[S^1(y_1, y_2) S^2(-y_1, -y_2) + S^2(y_1, y_2) S^1(-y_1, -y_2) \right] + \beta^4 S^2(y_1, y_2) S^2(-y_1, -y_2) \right\} \quad (3.14)$$

where

$$\mathcal{K} = \int d^2 b \left(G^{\text{dressed}}(Y, b) \right)^2 \bigg/ \left(\int d^2 b G^{\text{dressed}}(Y, b) \right)^2 \quad (3.15)$$

where $G^{\text{dressed}}(Y, b)$ is determined by Eq. (2.1) and Eq. (2.2). The contributions of enhanced diagrams are proportional to the square of the ratios given by Eq. (3.6) and, therefore, they are negligibly small.

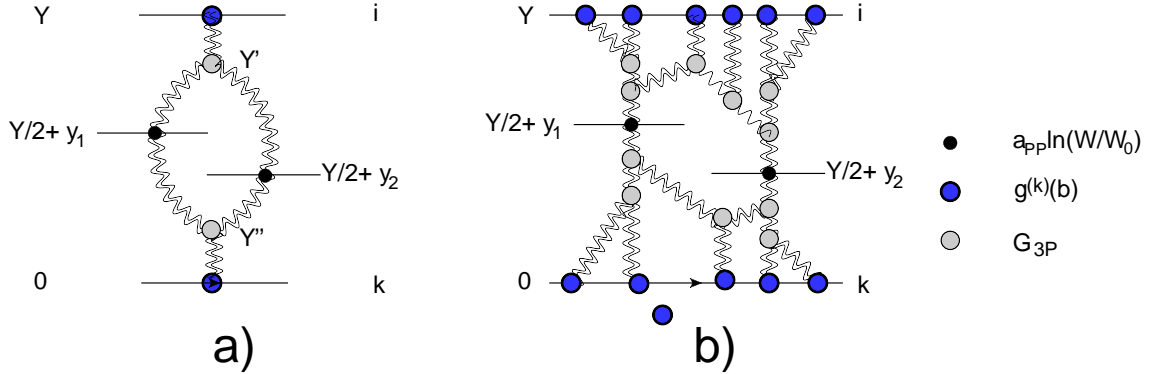


Figure 7. Mueller diagrams for the rapidity correlation between two particles produced in one parton showers: enhanced diagrams. Fig. 7-a shows the first Mueller diagram, while Fig. 7-b indicates the structure of general diagrams. The double wavy lines describe dressed BFKL Pomeron. The blobs stand for the vertices which are shown in the legend

3.4 Correlation function

The correlation function $R(y_1, y_2)$ is defined as

$$R(y_1, y_2) = \sigma_{NSD} \left\{ \frac{d^2 \sigma^{\text{2 parton showers}}}{dy_1 dy_2} + \frac{d^2 \sigma_{\text{semi-enhanced}}^{\text{1 parton shower}}}{dy_1 dy_2} + \frac{d^2 \sigma_{\text{enhanced}}^{\text{1 parton shower}}}{dy_1 dy_2} \right\} \bigg/ \left\{ \frac{d\sigma}{dy_1} \frac{d\sigma}{dy_2} \right\} - 1 \quad (3.16)$$

3.5 Kinematic corrections

In all our previous equations we assumed that $Y = \ln(W^2/W_0^2)$ with $W_0 = 1 \text{ GeV}$. This assumption appears natural for the elastic amplitude, and the cross section of the single inclusive production, but it should be re-examined for the correlation function. For this observable, the definition of Y has to be modified to account for the fact, that the energy of the parton shower is not equal to $W = \sqrt{s}$ ($s = W^2$), but it is smaller or equal to $\tilde{s} = \tilde{W}^2 = x_1 x_2 s = x_1 x_2 W^2$ (see Fig. 8, where we show the diffractive cut of the Mueller diagram of Fig. 4-a). The simplest way to find x_1 and x_2 is to assume that both

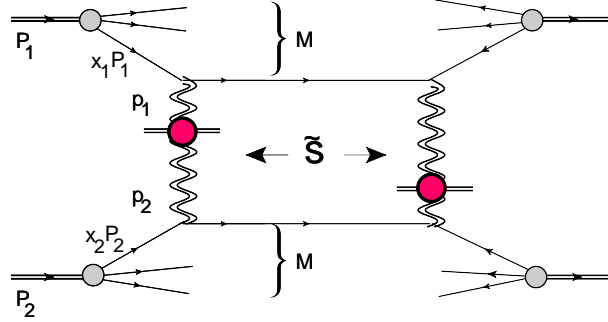


Figure 8. The Mueller diagram for the rapidity correlation between two particles produced in two parton showers: the diffractive cut of the diagram. The double wavy lines describe dressed BFKL Pomerons. The blob stands for a_{PP} .

$p_1^2 = p_2^2 = -\bar{Q}^2 \gg \mu_{\text{soft}}^2$, where μ_{soft} is the scale of the soft interactions, $\mu_{\text{soft}} \sim \Lambda_{QCD}$. In our approach the scale of hardness for the BFKL Pomeron $\bar{Q} = m \gg \mu_{\text{soft}}$. Bearing this in mind, the energy variable x_1 (x_2) for gluon-hadron scattering is equal to

$$0 = (x_1 P_1 + p_1)^2 = -\bar{Q}^2 + x_1 2 p_1 \cdot P_1; \quad p_1^2 = -\bar{Q}^2; \quad x_1 = \frac{\bar{Q}^2}{M^2 + \bar{Q}^2}. \quad (3.17)$$

p_1 , P_1 and $x_1 P_1$ are the momenta of the gluon, the hadron and the parton (quark or gluon) with which the initial gluon interacts. From Eq. (3.17) one has that

$$\tilde{s} = x_1 x_2 S = \frac{s \bar{Q}^4}{M^4} \quad (3.18)$$

where M denotes the mass of produced hadron in the diffractive process. For the two channel model, it is the mass of the diffractive state. We can use the quark structure function to estimate the typical value of $x_1 = x_2$ as it is suggested in Ref.[44]. Using the structure functions at $Q^2 \approx 25 \text{ GeV}^2$ one finds that $\langle |x_1| \rangle \approx 0.3 \div 0.5$. In Fig. 9 the values of $R(Y, 0, 0)$ are plotted for $Y = \ln(x_1^2 W^2/W_0^2)$ as function of x_1 .

3.6 Correlation in one parton shower: emission from one BFKL Pomeron

In addition to the sources of correlation that have been discussed above, we need to take into account the correlation between two gluons emitted from one BFKL Pomeron (see Fig. 10). At large $y_{12} = |y_1 - y_2|$

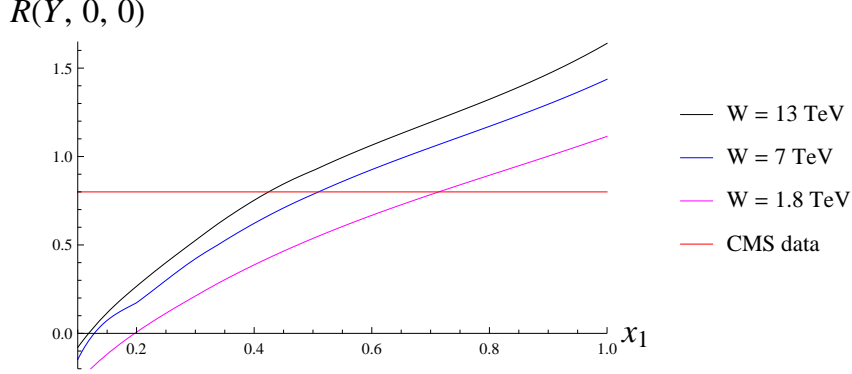


Figure 9. $R(Y, 0, 0)$ versus x_1 for $Y = \ln(x_1^2 W^2 / W_0^2)$ for different energies W . The red line indicates the moment $C_2 = \langle |n^2| \rangle / (\langle |n^2| \rangle)^2 = 2$ for the window in rapidity $-0.5 < y < +0.5$, measured by the CMS experiment [8].

the diagram of Fig. 10 induces long range correlations in rapidity, however, at small y_{12} this emission is suppressed, and we do not expect a large contribution from this source.

The contribution of this diagram can be written in the form

$$R^{\text{BFKL}}(y_1, y_2) = \frac{\sum_{i,k=1}^2 \alpha_i \alpha_k \Gamma_i(\frac{1}{2}Y - y_1) \tilde{G}^{\text{dressed}}(y_{12}) \Gamma_k(\frac{1}{2}Y + y_2)}{\sigma_{NSD} \sum_{i,k=1}^2 \alpha_i \alpha_k \Gamma_i(\frac{1}{2}Y - y_1) \Gamma_k(\frac{1}{2}Y + y_1) \sum_{i,k=1}^2 \alpha_i \alpha_k \Gamma_i(\frac{1}{2}Y - y_2) \Gamma_k(\frac{1}{2}Y + y_2)} \quad (3.19)$$

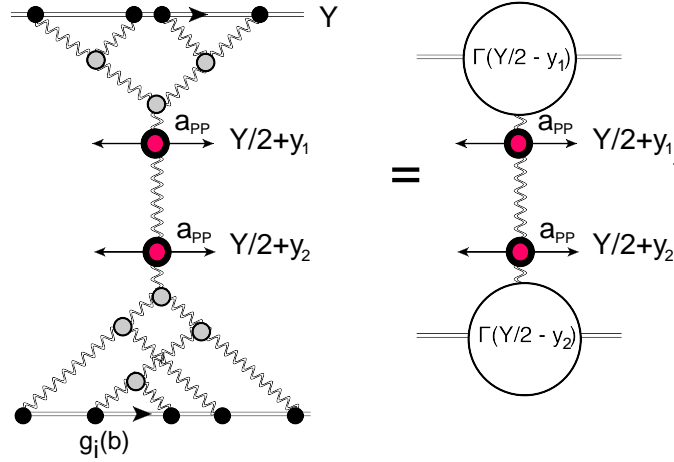


Figure 10. Mueller diagram for emission of particles from one BFKL Pomeron.

where

$$\Gamma_i(y) = \int d^2b N^{BK} \left(g_i(b) \tilde{G}^{\text{dressed}}(y) \right) \quad (3.20)$$

For small values of the argument $\Gamma_i(y) \xrightarrow{y \ll 1} \int d^2b g_i(b) \tilde{G}^{\text{dressed}}(y)$ Eq. (3.19), has no dependence on y_{12} , leading to long range rapidity correlations. However, it turns out that the exact computation, leads to very small values of $R^{\text{BFKL}}(y_1, y_2)$: approximately $0.2 \div 0.4$ % of the contributions from the sources discussed above.

3.7 Short range rapidity correlation

Besides long range rapidity correlations, the emission from one BFKL Pomeron, as well as the hadronization in one gluon jet, can lead to short range correlations in rapidity. Unfortunately, at present, this contribution cannot be treated on pure theoretical grounds, as it involves, confinement effects. To estimate this contribution, we introduce the Mueller diagram, shown in Fig. 11, where we describe this correlation by the phenomenological constant a_{PR} , and introduce the correlation length $\Delta \approx 2$. In the diagram of Fig. 11 for the zigzag line we have $a_{PR}^2 \exp(-\frac{y_{12}}{\Delta})$ ($y_{12} = |y_1 - y_2|$). Our estimate for Δ stems from Reggeon phenomenology, in which the zigzag line describes the contribution of the secondary Reggeon, with a propagator $\exp(-(1 - \alpha_R(0))y_{12})$ and $\alpha_R(0) \approx 0.5$.

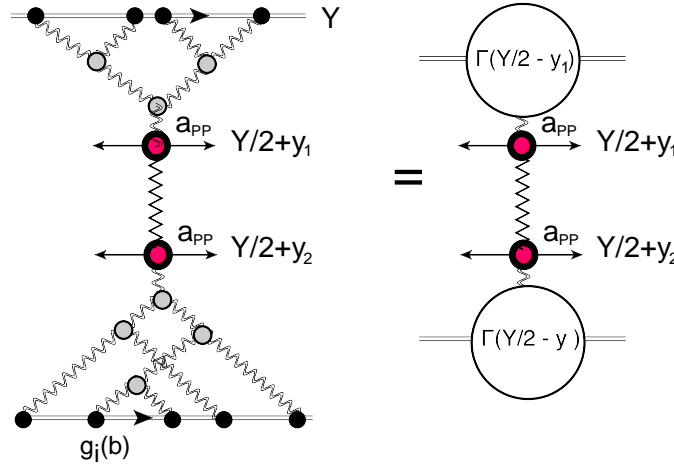


Figure 11. Mueller diagram for the short range rapidity correlations. Wavy double lines denote BFKL Pomerons, zigzag lines describe the exchange of the secondary Reggeon trajectory.

The contribution of this diagram takes the form

$$R^{\text{short range}}(y_1, y_2) = \left(\frac{a_{PR}}{a_{PP}} \right)^2 \sigma_{NSD} \frac{\sum_{i,k=1}^2 \alpha_i \alpha_k \Gamma_i \left(\frac{1}{2}Y - y_1 \right) e^{-\frac{y_{12}}{\Delta}} \Gamma_k \left(\frac{1}{2}Y + y_2 \right)}{\sum_{i,k=1}^2 \alpha_i \alpha_k \Gamma_i \left(\frac{1}{2}Y - y_1 \right) \Gamma_k \left(\frac{1}{2}Y + y_1 \right) \sum_{i,k=1}^2 \alpha_i \alpha_k \Gamma_i \left(\frac{1}{2}Y - y_2 \right) \Gamma_k \left(\frac{1}{2}Y + y_2 \right)} \quad (3.21)$$

4 Predictions and comparison with the experiment

Fig. 9, shows that the correlation function increases with energy, and becomes rather large (of the order of 1) at $W = 7 TeV$. This qualitative feature is in agreement with the experimental data from the LHC. The

first set of data, is the multiplicity distribution measured by the CMS collaboration[8]. In particular, the value of $C_2 = \langle |n^2| \rangle / (\langle |n^2| \rangle)^2$ turns out to be very close to 2, for the window in rapidities $-0.5 < \eta < 0.5$. Since $C_2 = R(0, 0) + 1 + 1/dN/d\eta|_{\eta=0}$ where $dN/d\eta|_{\eta=0}$ denotes the multiplicity at $\eta = 0$, and at $W = 7 TeV$ it is equal to 5.8, while $R(0, 0) = 0.82^*$.

The second set of the data is the measurement of the double parton interaction (DPI)[45]. In the LHC experiments, the double inclusive cross sections of two pairs of back-to-back jets with momenta $p_{T,1}$ and $p_{T,2}$, were measured with rapidities of two pairs (y_1 and y_2) close to each other ($y_1 \approx y_2$). These pairs can only be produced from two different parton showers. The data were parameterized in the form

$$\frac{d\sigma}{dy_1 d^2 p_{T,1} dy_2 d^2 p_{T,2}} = \frac{m}{2\sigma_{eff}} \frac{d\sigma}{dy_1 d^2 p_{T,1}} \frac{d\sigma}{dy_2 d^2 p_{T,2}} \quad (4.1)$$

where $m = 2$ for pairs of different jets, and $m = 1$ for identical pairs. One can calculate the rapidity correlation function using Eq. (4.1)

$$R(y_1, y_2, p_{T,1}, p_{T,2}) = \frac{\frac{1}{\sigma_{in}} \frac{d\sigma}{dy_1 d^2 p_{T,1} dy_2 d^2 p_{T,2}}}{\frac{1}{\sigma_{in}} \frac{d\sigma}{dy_1 d^2 p_{T,1}} \frac{1}{\sigma_{in}} \frac{d\sigma}{dy_2 d^2 p_{T,2}}} - 1 = \frac{\sigma_{in}}{\sigma_{eff}} - 1 \approx 2 \quad (4.2)$$

For the above the estimates we use $\sigma_{eff} = 12 - 15$ mb (see Refs. [45]) and $\sigma_{in} = \sigma_{tot} - \sigma_{el} - \sigma_{sd} - \sigma_{dd} \approx 50$ mb for the energy $W = 7 TeV$ (see Ref.[12] and references therein). These data confirm that at high energies we are dealing with a system of partons that have a large mutual attraction. The fact that we predict a smaller correlation than in this experiment, does not discourage us, since the correlation function in Eq. (4.2) differs from the one that we calculate (see Eq. (1.2)).

The forward-backward correlation has been measured by the ATLAS collaboration in Ref.[9]. The observable that was used in Ref.[9], differs from the correlation function $R(\eta_1, \eta_2)$, and it can be re-written as

$$\rho_{fb}^n = \frac{R(\eta_1, \eta_2)}{\sqrt{R(\eta_1, \eta_1) R(\eta_2, \eta_2)}} \quad (4.3)$$

The value of $\rho_{fb}^n \sim 0.666$ [9] indicates large correlations, but it is difficult to compare ρ_{fb}^n with our estimates, since ATLAS introduced a specific selection: the p_T of all produced particles should be larger than 500 MeV, while $R(\eta_1, \eta_2)$ is defined as integrated over all momenta.

Using $R(0, 0)$, we estimate the values for C_2 for $W = 13 TeV$, and using the formula for the negative binomial distribution:

$$\frac{\sigma_n}{\sigma} = \left(\frac{r}{\bar{n} + r} \right)^r \frac{\Gamma(n+r)}{n! \Gamma(r)} \left(\frac{\bar{n}}{\bar{n} + r} \right)^n \quad (4.4)$$

we obtain the multiplicity distribution in the rapidity window $-0.5 < \eta < 0.5$ shown in Fig. 12. In Eq. (4.4) $\bar{n} = dN/d\eta|_{\eta=0}$ which was calculated in our paper [13]. From Fig. 12 we expect a violation of the KNO scaling behavior[46]. Accordingly to KNO scaling $\sigma_n/\sigma = F(n/\bar{n})$ with $\bar{n} = \int_{-0.5}^{0.5} d\eta dN/d\eta = dN/d\eta|_{\eta=0}$.

*In this section we use pseudo rapidity η instead of rapidity y , since this variable is used to display data from LHC experiments. We recalculate $\eta = h(y)$ where function h is taken from our paper [13].

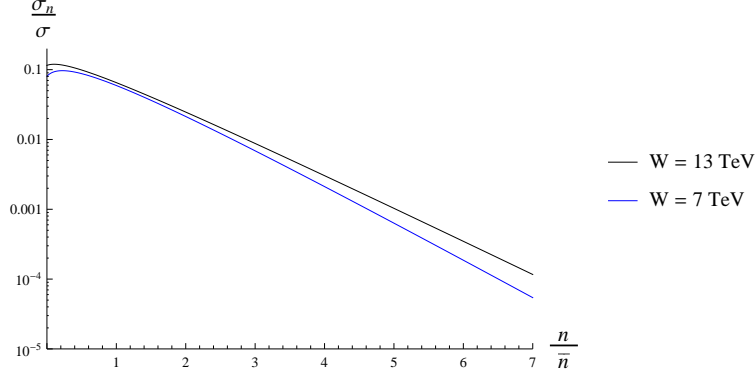


Figure 12. σ_n/σ versus multiplicity n/\bar{n} at different energies W in the rapidity window $-0.5 < y < 0.5$.

It turns out that $R(y_1, y_2)$ at fixed energy, depends neither on y_1 nor on y_2 , giving a perfect example of long range correlations in rapidity. To understand why we have these features, it is instructive to start from Fig. 4-a at small values of Y . In this kinematic region we can replace $\tilde{G}^{\text{dressed}} \rightarrow \tilde{G}^{\text{bare}} = \tilde{T}(Y)$ and $N^{BK}(Y, b) \rightarrow g_i(b) \tilde{G}^{\text{bare}}$. After simple algebra, the correlation function is equal to

$$R(y_1, y_2) = \frac{1}{\alpha^4} \sigma_{NSD} \frac{\left(\int d^2b \left(\int d^2b' g_1(\vec{b}) g_1(\vec{b} - \vec{b}') \right)^2 \right)}{\left(\int d^2b d^2b' g_1(\vec{b}) g_1(\vec{b} - \vec{b}') \right)^2} - 1 \quad (4.5)$$

In Eq. (4.5) we use the fact that in our model $g_1 \gg g_2$. Eq. (4.5) leads to a correlation function that does not depend on y_1 and y_2 .

On the other hand, at very large Y , $N^{BK}(Y, b) \rightarrow \Theta(R(Y) - b)$, where $\Theta(b)$ is a step function. Plugging in this simple expression, we obtain

$$\begin{aligned} R(y_1, y_2) &= \sigma_{NSD} \frac{\int d^2b \Theta(R(\tfrac{1}{2}Y - y_2) - b) \Theta(R(\tfrac{1}{2}Y - y_1) - b) R^2(\tfrac{1}{2}Y - y_1) R^2(\tfrac{1}{2}Y - y_2)}{\pi^2 R^4(\tfrac{1}{2}Y - y_1) R^4(\tfrac{1}{2}Y - y_2)} - 1 \\ &\rightarrow \frac{\sigma_{NSD}}{\pi R^2(\tfrac{1}{2}Y - y_1) \Big|_{y_1 < y_2}} - 1 \end{aligned} \quad (4.6)$$

$R(Y)$ in Eq. (4.6) denotes a typical impact parameter at large Y , which is proportional to Y^\dagger . Recall, that at high energies, all components of the wave functions in the two channel model, give the same contribution. This is the reason why we do not have an extra factor which depend on α and β .

Eq. (4.6) shows the logarithmic dependence on y_1 . Using Eq. (4.6) we can estimate the $y_1(y_2)$ dependence of $R(y_1, y_2)$ calculating

$$\langle |b^2(Y)| \rangle = \frac{\int b^2 d^2b N^{BK} \left(g_i(b) \tilde{G}^{\text{dressed}}(Y) \right)}{\int d^2b N^{BK} \left(g_i(b) \tilde{G}^{\text{dressed}}(Y) \right)} \quad (4.7)$$

[†]We trust that our use of the same notation for the correlation function and typical b , will not confuse the reader

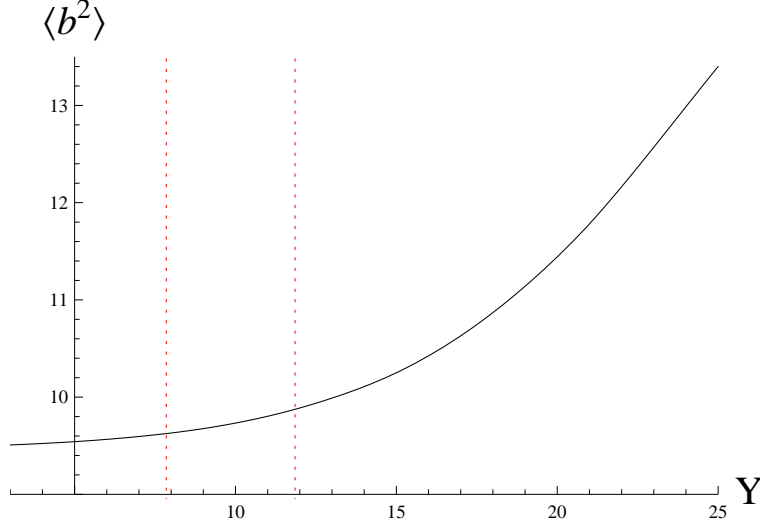


Figure 13. $\langle b^2(Y) \rangle$, defined in Eq. (4.7), versus Y .

From Fig. 13, in which we plot the results of our calculation, one can see, that only at large $Y > 11$ does $\langle b^2(Y) \rangle$ start showing visible Y dependence. Two vertical dotted lines mark the widow in rapidity, which is essential in the calculation of the correlation function at $W = 7 \text{ TeV}$ for $-2 < y_1, y_2 < 2$. We can expect a change of R by 2%. The actual calculation gives even less. Using $N^{BK}(Y, b) \rightarrow \Theta(R(Y) - b)$ gives $R^2(Y) = 2\langle b^2(Y) \rangle$. Using this relation, we estimate $R(y_1, y_2)$ as

$$R(y_1, y_2) = \frac{1}{\alpha^4} \frac{\sigma_{NSD}}{2\pi \langle b^2(\frac{1}{2}Y - y_1) \rangle} - 1 \quad (4.8)$$

At $W = 7 \text{ TeV}$ from Eq. (4.8) we find that $R(y_1, y_2) = 1.647$, while the exact calculation give 1.437 (see Fig. 9). At $W = 13 \text{ TeV}$ this simple formula leads to $R(y_1, y_2) = 1.72$, versus 1.64 from the exact calculations (see Fig. 9).

The correlations, measured by the ATLAS collaboration[9], at first sight contradict both our estimate and the CMS data, regarding the multiplicity distribution. We first check Eq. (4.3). The measured observable has the form [9]

$$\rho_{fb}^n = \frac{\langle (n_f - \langle n_f \rangle) (n_b - \langle n_b \rangle) \rangle}{\sqrt{\langle (n_f - \langle n_f \rangle)^2 \rangle \langle (n_b - \langle n_b \rangle)^2 \rangle}} \quad (4.9)$$

The numerator of Eq. (4.9) can be written as $R(y_1, y_2) \Delta y_1 \Delta y_2$, where Δy_i is the interval of rapidities where the hadrons are measured. However, at the same value of rapidity $R(y_1, y_1) (\Delta y_1)^2$ corresponds to $\langle n(n-1) \rangle - \langle n \rangle^2$. Therefore, the expression for

$$\langle (n_f - \langle n_f \rangle)^2 \rangle = \left(R(y_1, y_1) + \frac{1}{\frac{dN}{dy_1} \Delta y_1} \right) (\Delta y_1)^2$$

which leads to the following formula for ρ_{fb}^n :

$$\rho_{fb}^n = \frac{R(y_1, y_2)}{\sqrt{\left(R(y_1, y_1) + \frac{1}{\frac{dN}{dy_1} \Delta y_1}\right) \left(R(y_2, y_2) + \frac{1}{\frac{dN}{dy_2} \Delta y_2}\right)}} \quad (4.10)$$

Taking $\Delta y_1 = 0.5$, we see that the first element of the Table 2 is equal to 0.7, which is in good agreement with the experimental value 0.666 ± 0.011 .

Forward η interval Backward η interval	0.0 – 0.5	0.5 – 1.0	1.0 – 1.5	1.5 – 2.0	2.0 – 2.5
0.0 – 0.5	0.666 (0.70) ± 0.011	0.624(0.643) ± 0.011	0.592 (0.599) ± 0.011	0.566 (0.565) ± 0.012	0.540 (0.539) ± 0.013
0.5 – 1.0	0.624 (0.667) ± 0.011	0.596(0.618) ± 0.011	0.574 (0.580) ± 0.012	0.553 (0.550) ± 0.013	0.530 (0.527) ± 0.014
1.0 – 1.5	0.594 (0.640) ± 0.011	0.576(0.596) ± 0.012	0.560 (0.563) ± 0.013	0.540 (0.537) ± 0.014	0.518 (0.516) ± 0.014
1.5 – 2.0	0.571(0.615) ± 0.012	0.557(0.577) ± 0.013	0.544(0.548) ± 0.014	0.526 (0.525) ± 0.014	0.503 (0.508) ± 0.016
2.0 – 2.5	0.551 (0.593) ± 0.013	0.540 (0.560) ± 0.014	0.527 (0.535) ± 0.014	0.507(0.515) ± 0.016	0.487(0.499) ± 0.018

Table 2. Multiplicity correlations for events at $\sqrt{s} = 7$ TeV for events with a minimum of two charged particles in the kinematic interval $p_T > 100$ MeV and $|\eta| < 2.5$ for different combinations of forward and backward pseudorapidity interval. The data is take from Ref.[9]. The numbers in parentheses are our estimates.

To describe our results given in Table 2, we need to also take short range rapidity correlations into account. In this table, in parenthesis, we have our estimates, which we obtain on describing the correlation function in the form

$$R(y_1, y_2) = R^{\text{long range}}(y_1, y_2) + \left(R^{\text{short range}}(y_1, y_2) - R^{\text{short range}}(0, 0) \right); \quad (4.11)$$

$$R^{\text{short range}}(y_1, y_2) = a \frac{\Gamma_1\left(\frac{1}{2}Y - y_1\right) e^{-\frac{y_{12}}{\Delta}} \Gamma_1\left(\frac{1}{2}Y + y_2\right)}{\Gamma_1\left(\frac{1}{2}Y - y_1\right) \Gamma_1\left(\frac{1}{2}Y + y_1\right) \Gamma_1\left(\frac{1}{2}Y - y_2\right) \Gamma_1\left(\frac{1}{2}Y + y_2\right)}$$

with $a = 0.7$ and $\Delta = 2$. In Eq. (4.11) $y_{12} = |y_1 - y_2|$ and we restrict ourself by the contribution of the state "1" in Eq. (3.21), since $g_1 \gg g_2$. We assumed that $R^{\text{short range}}(0, 0) = 0$ since at $y_{12} = 0$ Eq. (3.21) leads to the long range correlations which we have calculated in section 3.4. One can see that the agreement is not perfect, but it demonstrates that the ATLAS data can be reproduced, by including the short range correlations.

5 Conclusion

The main result of this paper is that in our model, which is based on the CGC/saturation approach, we have discovered a mechanism that produces large, long range rapidity correlations at high energies. The large values of the correlation function $R(y_1, y_2) \geq 1$ at high energies, lends strong support to the idea, that at high energies the system of partons that is produced, is not only dense, but also has strong attractive forces acting between the partons. The resulting long range rapidity correlations are independent of $y_{1,2}$. This prediction is in direct contradiction to the estimates from the soft Pomeron based model that we made (see Ref.[43]). In that model the correlations from one parton shower are larger than from the two parton showers, and they led to the $y_{1,2}$ dependence. Scrutinizing our formulae we found that the main reason for the smallness of the correlation in one parton shower that we observed in our approach, stems from the most theoretically reliable part of our model: from the expression for the dressed BFKL Pomeron Green function.

We demonstrated that our model is able to describe the LHC data, emanating from the CMS and ATLAS collaborations. These data are certainly insufficient for a thorough analysis of the details of our approach, but they confirm that the long range rapidity correlations are large at high energies. The prediction for $W = 13 \text{ TeV}$ is shown in Fig. 9. The correlations should increase with the energy and the results measurements at $W = 13 \text{ TeV}$ will clarify the situation.

In general we believe that this paper is the next natural step, in building a model capable of describing soft high energy interactions based on the CGC/saturation approach.

6 Acknowledgements

We thank our colleagues at Tel Aviv university and UTFSM for encouraging discussions. Our special thanks go to Carlos Cantreras, Alex Kovner and Misha Lublinsky for elucidating discussions on the subject of this paper. This research was supported by the BSF grant 2012124 and by the Fondecyt (Chile) grant 1140842.

References

- [1] M. G. Poghosyan, J. Phys. G G **38**, 124044 (2011) [arXiv:1109.4510 [hep-ex]]. ALICE Collaboration, “*First proton–proton collisions at the LHC as observed with the ALICE detector: measurement of the charged particle pseudorapidity density at $\sqrt{s} = 900 \text{ GeV}$,*” arXiv:0911.5430 [hep-ex].
- [2] G. Aad *et al.* [ATLAS Collaboration], Nature Commun. **2**, 463 (2011) [arXiv:1104.0326 [hep-ex]].
- [3] CMS Physics Analysis Summary: “Measurement of the inelastic pp cross section at $\sqrt{s} = 7 \text{ TeV}$ with the CMS detector”, 2011/08/27.
- [4] F. Ferro [TOTEM Collaboration], AIP Conf. Proc. **1350**, 172 (2011) ; G. Antchev *et al.* [TOTEM Collaboration], Europhys. Lett. **96**, 21002 (2011), **95**, 41001 (2011) [arXiv:1110.1385 [hep-ex]]; G. Antchev *et al.* [TOTEM Collaboration], Phys. Rev. Lett. **111** (2013) 26, 262001 [arXiv:1308.6722 [hep-ex]].
- [5] ALICE Collaboration, Eur. Phys. J. C **65** (2010) 111 [arXiv:0911.5430 [hep-ex]].

- [6] S. Chatrchyan *et al.* [CMS and TOTEM Collaborations], *Eur. Phys. J. C* **74** (2014) 10, 3053 [arXiv:1405.0722 [hep-ex]]; V. Khachatryan *et al.* [CMS Collaboration], *JHEP* **1002** (2010) 041 [arXiv:1002.0621 [hep-ex]].
- [7] ATLAS Collaboration, arXiv:1003.3124 [hep-ex].
- [8] V. Khachatryan *et al.* [CMS Collaboration], *JHEP* **1101** (2011) 079 [arXiv:1011.5531 [hep-ex]].
- [9] G. Aad *et al.* [ATLAS Collaboration], *JHEP* **1207** (2012) 019 [arXiv:1203.3100 [hep-ex]].
- [10] Yuri V Kovchegov and Eugene Levin, “ *Quantum Chromodynamics at High Energies*”, Cambridge Monographs on Particle Physics, Nuclear Physics and Cosmology, Cambridge University Press, 2012 .
- [11] E. Gotsman, E. Levin and U. Maor, *Eur. Phys. J. C* **75** (2015) 1, 18 [arXiv:1408.3811 [hep-ph]].
- [12] E. Gotsman, E. Levin and U. Maor, *Eur. Phys. J. C* **75** (2015) 5, 179 [arXiv:1502.05202 [hep-ph]].
- [13] E. Gotsman, E. Levin and U. Maor, *Phys. Lett. B* **746** (2015) 154 [arXiv:1503.04294 [hep-ph]].
- [14] L. V. Gribov, E. M. Levin and M. G. Ryskin, *Phys. Rep.* **100** (1983) 1.
- [15] A. H. Mueller and J. Qiu, *Nucl. Phys.* **B268** (1986) 427.
- [16] L. McLerran and R. Venugopalan, *Phys. Rev.* **D49** (1994) 2233, 3352; **D50** (1994) 2225; **D53** (1996) 458; **D59** (1999) 09400.
- [17] I. Balitsky, [arXiv:hep-ph/9509348]; *Phys. Rev.* **D60**, 014020 (1999) [arXiv:hep-ph/9812311]
- [18] A. H. Mueller, *Nucl. Phys.* **B415** (1994) 373; **B437** (1995) 107.
- [19] Y. V. Kovchegov, *Phys. Rev.* **D60**, 034008 (1999), [arXiv:hep-ph/9901281].
- [20] J. Jalilian-Marian, A. Kovner, A. Leonidov and H. Weigert, *Phys. Rev.* **D59**, 014014 (1999), [arXiv:hep-ph/9706377]; *Nucl. Phys.* **B504**, 415 (1997), [arXiv:hep-ph/9701284]; J. Jalilian-Marian, A. Kovner and H. Weigert, *Phys. Rev.* **D59**, 014015 (1999), [arXiv:hep-ph/9709432]; A. Kovner, J. G. Milhano and H. Weigert, *Phys. Rev.* **D62**, 114005 (2000), [arXiv:hep-ph/0004014]; E. Iancu, A. Leonidov and L. D. McLerran, *Phys. Lett.* **B510**, 133 (2001); [arXiv:hep-ph/0102009]; *Nucl. Phys.* **A692**, 583 (2001), [arXiv:hep-ph/0011241]; E. Ferreiro, E. Iancu, A. Leonidov and L. McLerran, *Nucl. Phys.* **A703**, 489 (2002), [arXiv:hep-ph/0109115]; H. Weigert, *Nucl. Phys.* **A703**, 823 (2002), [arXiv:hep-ph/0004044].
- [21] D. Kharzeev, E. Levin and M. Nardi, *Nucl. Phys. A* **730** (2004) 448 [Erratum-ibid. A **743** (2004) 329] [arXiv:hep-ph/0212316]; *Phys. Rev. C* **71** (2005) 054903 [arXiv:hep-ph/0111315]; D. Kharzeev and E. Levin, *Phys. Lett. B* **523** (2001) 79 [arXiv:nucl-th/0108006]; D. Kharzeev and M. Nardi, *Phys. Lett. B* **507** (2001) 121 [arXiv:nucl-th/0012025].
- [22] D. Kharzeev, E. Levin and M. Nardi, *Nucl. Phys. A* **747** (2005) 609 [arXiv:hep-ph/0408050].
- [23] E. Levin and A. H. Rezaeian, *AIP Conf. Proc.* **1350** (2011) 243 [arXiv:1011.3591 [hep-ph]]; *Phys. Rev. D* **82** (2010) 014022 [arXiv:1005.0631 [hep-ph]]; [arXiv:1102.2385 [hep-ph]]; *Phys. Rev. D* **82** (2010) 054003. [arXiv:1007.2430 [hep-ph]].
- [24] L. McLerran, M. Praszalowicz, *Nucl. Phys. A* **916** (2013) 210 [arXiv:1306.2350 [hep-ph]]; *Acta Phys. Polon.* **B42** (2011) 99 [arXiv:1011.3403 [hep-ph]]; *Acta Phys. Polon.* **B41** (2010) 1917. [arXiv:1006.4293 [hep-ph]].
- [25] M. Praszalowicz, *Phys. Lett. B* **727** (2013) 461 [arXiv:1308.5911 [hep-ph]]; *Acta Phys. Polon. Supp.* **6** (2013) 3, 809 [arXiv:1304.1867 [hep-ph]]; *Phys. Lett. B* **704** (2011) 566 [arXiv:1101.6012 [hep-ph]]; *Phys. Rev. Lett.* **106** (2011) 142002 [arXiv:1101.0585 [hep-ph]].

- [26] E. A. Kuraev, L. N. Lipatov, and F. S. Fadin, *Sov. Phys. JETP* **45**, 199 (1977); Ya. Ya. Balitsky and L. N. Lipatov, *Sov. J. Nucl. Phys.* **28**, 22 (1978).
- [27] L. N. Lipatov, *Phys. Rep.* **286** (1997) 131; *Sov. Phys. JETP* **63** (1986) 904 and references therein.
- [28] A. H. Mueller and B. Patel, *Nucl. Phys.* **B425** (1994) 471.
- [29] J. Bartels, M. Braun and G. P. Vacca, *Eur. Phys. J.* **C40** (2005) 419 [arXiv:hep-ph/0412218]. J. Bartels and C. Ewerz, *JHEP* **9909** 026 (1999) [arXiv:hep-ph/9908454]. J. Bartels and M. Wusthoff, *Z. Phys.* **C6**, (1995) 157. J. Bartels, *Z. Phys.* **C60** (1993) 471.
- [30] M. A. Braun, *Phys. Lett.* **B632** (2006) 297 [arXiv:hep-ph/0512057]; *Eur. Phys. J.* **C16** (2000) 337 [arXiv:hep-ph/0001268]; *Phys. Lett.* **B483** (2000) 115 [arXiv:hep-ph/0003004]; *Eur. Phys. J.* **C33** (2004) 113 [arXiv:hep-ph/0309293]; **C6**, 321 (1999) [arXiv:hep-ph/9706373]. M. A. Braun and G. P. Vacca, *Eur. Phys. J.* **C6** (1999) 147 [arXiv:hep-ph/9711486].
- [31] Y. V. Kovchegov and E. Levin, *Nucl. Phys. B* **577** (2000) 221 [hep-ph/9911523].
- [32] E. Levin and M. Lublinsky, *Nucl. Phys. A* **763** (2005) 172 [arXiv:hep-ph/0501173]; *Phys. Lett. B* **607** (2005) 131 [arXiv:hep-ph/0411121]; *Nucl. Phys. A* **730** (2004) 191 [arXiv:hep-ph/0308279].
- [33] E. Levin, J. Miller and A. Prygarin, *Nucl. Phys.* **A806** (2008) 245, [arXiv:0706.2944 [hep-ph]].
- [34] T. Altinoluk, C. Contreras, A. Kovner, E. Levin, M. Lublinsky and A. Shulkin, *Int. J. Mod. Phys. Conf. Ser.* **25** (2014) 1460025; T. Altinoluk, N. Armesto, A. Kovner, E. Levin and M. Lublinsky, *JHEP* **1408** (2014) 007; T. Altinoluk, A. Kovner, E. Levin and M. Lublinsky, *JHEP* **1404** (2014) 075 [arXiv:1401.7431 [hep-ph]].; T. Altinoluk, C. Contreras, A. Kovner, E. Levin, M. Lublinsky and A. Shulkin, *JHEP* **1309** (2013) 115.
- [35] E. Levin, *JHEP* **1311** (2013) 039 [arXiv:1308.5052 [hep-ph]].
- [36] P.D.B. Collins, *"An introduction to Regge theory and high energy physics"*, Cambridge University Press 1977.
- [37] A. H. Mueller, *Phys. Rev.* **D2** (1970) 2963.
- [38] A. H. Mueller and B. Patel, *Nucl. Phys.* **B425** (1994) 471. A. H. Mueller and G. P. Salam, *Nucl. Phys.* **B475**, (1996) 293. [arXiv:hep-ph/9605302]. G. P. Salam, *Nucl. Phys.* **B461** (1996) 512; E. Iancu and A. H. Mueller, *Nucl. Phys.* **A730** (2004) 460 [arXiv:hep-ph/0308315]; 494 [arXiv:hep-ph/0309276].
- [39] M. L. Good and W. D. Walker, *Phys. Rev.* **120** (1960) 1857.
- [40] V. A. Abramovsky, V. N. Gribov and O. V. Kancheli, *Yad. Fiz.* **18** (1973) 595 [*Sov. J. Nucl. Phys.* **18** (1974) 308].
- [41] J. Jalilian-Marian and Y. V. Kovchegov, *Phys. Rev. D* **70** (2004) 114017 [Erratum-ibid. *D* **71** (2005) 079901] [hep-ph/0405266]; *Prog. Part. Nucl. Phys.* **56** (2006) 104 [hep-ph/0505052].
- [42] E. Levin and A. Prygarin, *Phys. Rev. C* **78** (2008) 065202 [arXiv:0804.4747 [hep-ph]].
- [43] E. Gotsman, E. Levin and U. Maor, *Eur. Phys. J. C* **73** (2013) 2658 [arXiv:1307.4925 [hep-ph]].
- [44] E. Gotsman, E. Levin and U. Maor, *Phys. Rev. D* **87** (2013) 7, 071501 [arXiv:1302.4524 [hep-ph]].
- [45] G. Aad *et al.* [ATLAS Collaboration], *New J. Phys.* **15** (2013) 033038 [arXiv:1301.6872 [hep-ex]], V. M. Abazov *et al.* [D0 Collaboration], *Phys. Rev. D* **81** (2010) 052012 [arXiv:0912.5104 [hep-ex]], F. Abe *et al.* [CDF Collaboration], *Phys. Rev. D* **47** (1993) 4857, *Phys. Rev. D* **56** (1997) 3811, J. Alitti *et al.* [UA2

Collaboration], Phys. Lett. B **268** (1991) 145, T. Akesson *et al.* [Axial Field Spectrometer Collaboration], Z. Phys. C **34**, 163 (1987).

[46] Z. Koba, H. B. Nielsen, and P. Olesen, Nucl. Phys. B40 (1972) 317.

